

Dielectric function of zinc-blende AlN from 1 to 20 eV: Band gap and van Hove singularities

M. Röppischer,^{1,a)} R. Goldhahn,² G. Rossbach,² P. Schley,² C. Cobet,¹ N. Esser,¹ T. Schupp,³ K. Lischka,³ and D. J. As³

¹Department Berlin, ISAS—Institute for Analytical Sciences, Albert-Einstein-Str. 9, 12489 Berlin, Germany

²Institut für Physik, Technische Universität Ilmenau, PF 100565, 98684 Ilmenau, Germany

³Department of Physics, University of Paderborn, Warburger Str. 100, 33098 Paderborn, Germany

(Received 1 September 2009; accepted 3 September 2009; published online 12 October 2009)

The dielectric function (DF) of phase-pure cubic AlN films is determined by ellipsometry. The sharp onset of the imaginary part of the DF defines the direct absorption edge corresponding to a conduction-to-valence band spacing at the center of the Brillouin zone (BZ) of 5.93 eV. Phonon-assisted transitions lead to the pronounced absorption tail below this edge from which the indirect gap of zinc-blende AlN is estimated with 5.3 eV. Transitions due to four additional critical points of the BZ are resolved at higher photon energies. The high-frequency and static dielectric constants are determined with 4.25 and 8.07, respectively. © 2009 American Institute of Physics. [doi:10.1063/1.3239516]

Group-III nitride semiconductors with nonpolar zinc-blende (zb) structure exhibit some interesting properties making them attractive for the application in optoelectronic devices.¹ Most important, cubic heterostructures with (001) orientation do not suffer from strong built-in electric fields caused by spontaneous and piezoelectric polarization along the polar *c*-direction of the widely used wurtzite (wz) layers.² The suppression of the quantum confined Stark effect in low-dimensional cubic structures leads, e.g., to high emission efficiencies of AlGaIn/GaN quantum wells,¹ to long decay times of the exciton spin polarization for GaN/AlN quantum dots,³ or to a redshift of the near-infrared intersubband absorption of GaN/AlN superlattices.⁴

Although zb-AlN is nowadays used in heterostructures as barrier material, its band structure and optical properties are not well known yet. Calculations^{5–8} predict an indirect band (E_{ind}) gap at about 5 eV for which the absolute conduction band minimum is located at the *X*-point of the Brillouin zone (BZ). The direct gap (E_0 at the Γ -point) should be found about 800 meV higher in energy. Hexagonal inclusions and a comparably rough surface^{9,10} impeded so far a reliable experimental determination of both gaps. It was recently demonstrated,^{1,4,11,12} however, that the phase purity and structural properties of cubic InN and GaN can be considerably improved by growing on free-standing 3C-SiC(001) substrates. Likewise, high-quality zb-AlN layers can be expected by direct growth on 3C-SiC, in particular due to the almost identical lattice parameters of 4.38 (Ref. 10) and 4.36 Å,¹³ respectively. In this paper, the dielectric function (DF) from the infrared into the vacuum-ultraviolet region is reported for those films. The analysis yields unambiguously the transition energies of the direct gap and high-energy critical points (CPs) as well as clear evidence for an indirect band gap.

Here, the optical properties of two zb-AlN layers with thicknesses of 40 (T40) and 100 nm (T100) are reported. They were grown by rf plasma-assisted molecular beam epitaxy on free-standing 3C-SiC(001) substrates. *In situ* monitoring by reflection high-energy electron diffraction revealed a two-dimensional layer-by-layer growth mode while x-ray diffraction indicated pseudomorphic deposition onto the substrate and the cubic structure. Atomic force microscopy of $10 \times 10 \mu\text{m}^2$ areas yielded a root mean square roughness of 0.4 nm (T40) and 0.6 nm (T100). Thicker films show an increase in roughness caused by a transition to a more three-dimensional growth mode; they are therefore not included in this study. The conducting substrate and low layer thickness did not allow to determine the carrier concentration of the unintentionally doped films. Details of the growth procedure and more results of the structural characterization are published elsewhere.¹⁴

The ellipsometric parameters Ψ and Δ were recorded by a commercial ellipsometer in the photon energy ($\hbar\omega$) range from 1 to 6.4 eV at different angles of incidence (60°, 67°, and 74°). For $\hbar\omega > 5$ eV, we used a home made construction attached to the Berlin electron storage ring for synchrotron radiation (BESSY II) with the setup described in Ref. 15 (angle of incidence 67.5°). All measurements were carried out at room temperature. The real (ϵ_1) and imaginary (ϵ_2) parts of the complex DF ($\bar{\epsilon}$) of the zb-AlN layers are obtained by a multilayer fitting procedure of Ψ and Δ ,¹⁶ i.e., the remaining surface roughness is taken into account. No assumption was made concerning the shape of the DF, which means that ϵ_1 and ϵ_2 were separately fitted for every photon energy. The Kramers–Kronig consistency between ϵ_1 and ϵ_2 was proved in the final step of the data analysis.

Figure 1(a) shows the DF results for the two samples in the energy range up to 9.5 eV; spectral features of particular interest are labeled by E_0 , E_1 , and E_2 . Almost no difference is found in the spectral dependence for both films, only the magnitude around E_1 differs slightly. The excellent overall

^{a)}Electronic mail: roepischer@isas.de.

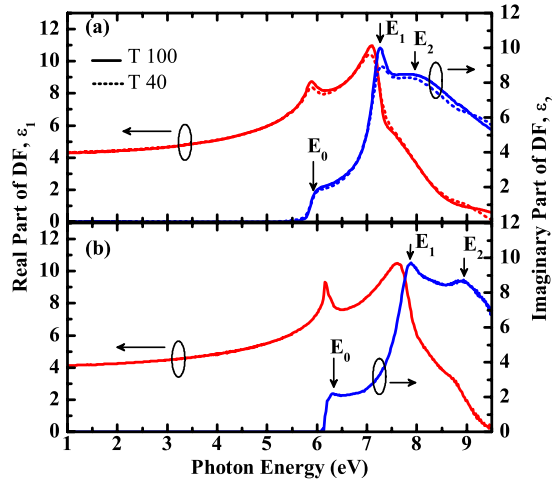


FIG. 1. (Color online) Comparison of the real and imaginary parts of the DF for zb-AIN (a) with the ordinary DF of wz-AIN (b). The dashed and solid lines in (a) are obtained for the films with 40 and 100 nm layer thicknesses, respectively.

agreement confirms the reproducibility of the growth procedure. The sharp onset of ϵ_2 above 5.88 eV is correlated with the direct band gap of zb-AIN, while E_1 and E_2 are attributed to transitions at other high-symmetry points of the BZ as analyzed in detail below.

Figure 1(b) shows for comparison the ordinary DF (Ref. 17) (electric field polarization perpendicular to the c -axis) of wz-AIN grown on 6H-SiC substrate. The similarities of the spectral dependence for both polymorphs are obvious, in particular the highest transition probability is found at the E_1 peak followed by a rather broad shoulder (E_2). The pronounced blueshift of E_0 , E_1 , and E_2 with respect to the cubic material should be noticed.

A magnification of ϵ_2 around the band gap for the two polymorphs is shown in Fig. 2. Previous studies¹⁷ of wz-GaN and wz-AIN demonstrated that two contributions have to be taken into account in order to determine the band gap at the Γ -point of the BZ. Surface electric fields (depletion region caused by surface states) broaden the discrete exciton lines below the gap¹⁸ while the plateaulike behavior above the gap is attributed to exciton continuum (Sommerfeld enhancement). Applying the analytical model for ϵ_2 from Ref. 17, which includes both contributions and adopting an exciton binding energy of 48 meV reported for wz-AIN,¹⁹ then the fit for zb-AIN yields the dashed line in Fig. 2. As the

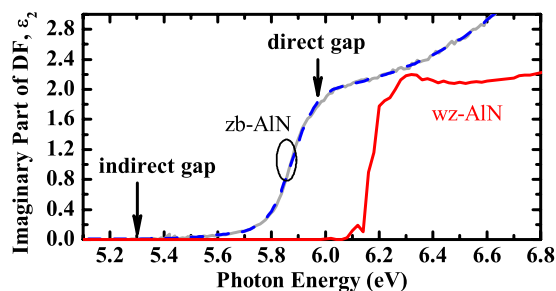


FIG. 2. (Color online) Imaginary part of the DF (solid lines) for zb-AIN (sample T100) and wz-AIN around the band gap. The dashed line represents the fit result for the cubic compound as explained in the text.

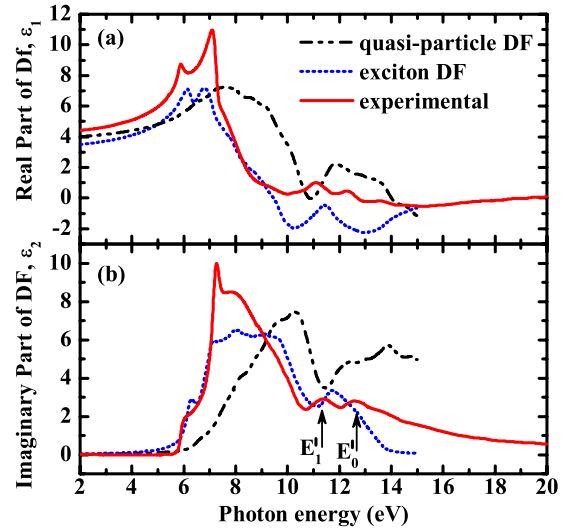


FIG. 3. (Color online) Comparison of the experimental DF for zb-AIN with the calculated results from Ref. 8. The real and imaginary parts are plotted in (a) and (b), respectively.

main result, the direct gap is determined with 5.93 eV, which is above the value of 5.74 eV estimated from investigations of mixed-phase AlN (Ref. 10) but below 6.05 eV extracted from reflectance measurements.²⁰ The calculated quasiparticle band gaps^{6–8} are very close to the experimental result.

Figure 2 demonstrates furthermore that cubic AlN exhibits in contrast to the hexagonal material a long absorption tail below the direct gap. The behavior is typical for phonon-assisted indirect absorption. The imaginary part of the DF differs appreciably from zero only above 5.3 eV, i.e., this energy defines the upper limit of the indirect band gap. A slightly lower value might be possible as well, but ellipsometry is not sensitive enough in the case of small absorption in combination with a low layer thickness. For comparison, Thompson *et al.*²¹ reported for the indirect band gap a value of 5.34 eV.

Studies of hexagonal GaN (Ref. 22) and InN (Ref. 23) revealed that DF calculations on the basis of the quasiparticle band structure alone are not sufficient in order to get the correct peak positions and intensity ratios for ϵ_2 . The inclusion of excitonic effects over the whole spectral range leads to redshift of the peak positions and a redistribution of oscillator strength. Figure 3 shows a comparison of the current experimental data for cubic AlN with the calculated quasiparticle and exciton DFs taken from Ref. 8, which include the lattice polarizability in addition. It is obvious that the inclusion of electron-hole interaction leads to a much better overall agreement.

In order to determine characteristic transition energies more precisely, the third derivative of the DF is analyzed within the joined density of state model;¹⁵ the ascertained energies are marked in Figs. 1(a) and 3. Note, a quantitative comparison with the calculated quasiparticle energies^{5–8} is not possible due to the exciton effects. The spectrum is dominated by the distinct peak at 7.204 eV (E_1) correlated with a CP around the X -point of the BZ. The E_2 transition at 7.95 eV is probably found along the [111]-direction. The energetic ordering of the E_1 and E_2 CPs is reversed in com-

parison to zb-GaN.¹⁵ The other two transition energies amount to 11.14 eV (E'_1) and 12.52 eV (E'_0) tentatively assigned to the L - and Γ -points of the BZ.

Finally, the dispersion of ε_1 in Fig. 1(a) for the transparent region ($\hbar\omega < 5$ eV) can be represented as for wz-AlN by the analytic expression²⁴

$$\varepsilon_1(\hbar\omega) = 1 + \frac{2}{\pi} \left(\frac{A_G}{2} \ln \frac{E_H^2 - (\hbar\omega)^2}{E_G^2 - (\hbar\omega)^2} + \frac{A_H E_H}{E_H^2 - (\hbar\omega)^2} \right),$$

in which E_G and E_H denote average energies of the band gap and the high-energy transitions, respectively, with the corresponding magnitudes A_G and A_H . For cubic AlN, one obtains $E_G=5.78$, $E_H=10.38$, $A_G=3.06$, and $A_H=34.28$ eV. The extrapolation to zero photon energy yields for the high-frequency dielectric constant ε_∞ a value of 4.25. The static dielectric constant ε_s is obtained via the Lyddane–Sachs–Teller relation $\varepsilon_s = (\omega_{LO}/\omega_{TO})^2 \varepsilon_\infty$ with the longitudinal and transversal optical phonon frequencies of 897 and 651 cm^{-1} from Ref. 25. It leads to a value of $\varepsilon_s=8.07$ for cubic AlN.

In summary, a detailed discussion of the optical properties of cubic AlN has been presented. In particular, the transition energy for the direct absorption was determined as well as a clear indication for the indirect band gap of the compound was found. The DF at high photon energies shows sharp transitions, which are correlated with CPs of the band structure.

This work was supported by the BMBF (Grant Nos. 05KS4KTB/3 and 05ES3XBA/5), the European commission within the seventh framework program (NanoCharM), the DFG graduate program “Micro- and Nanostructures in Optoelectronics and Photonics,” and the Thüringer Kultusministerium (EFRE, Grant No. B715-08015). D.J.A. wants to thank Dr. M. Abe and Dr. H. Nagasawa at HOYA Corporation for the supply of the excellent 3C-SiC substrates.

¹D. J. As, *Microelectron. J.* **40**, 204 (2009).

²R. Butté and N. Grandjean, in *Polarization Effects in Semiconductors: From Ab Initio Theory to Device Applications*, edited by C. Wood and D. Jena (Springer, New York, 2008), p. 467.

³D. Lagarde, A. Balocchi, H. Carrère, P. Renucci, T. Amand, X. Marie, S. Founta, and H. Mariette, *Phys. Rev. B* **77**, 041304 (2008).

⁴E. A. DeCuir, Jr., M. O. Manasreh, E. Tschumak, J. Schörmann, D. J. As, and K. Lischka, *Appl. Phys. Lett.* **92**, 201910 (2008).

⁵F. Litimein, B. Bouhafas, Z. Dridi, and P. Ruterana, *New J. Phys.* **4**, 64 (2002).

⁶F. Sökeland, M. Rohlfing, P. Krüger, and J. Pollmann, *Phys. Rev. B* **68**, 075203 (2003).

⁷A. Qteish, A. I. Al-Sharif, M. Fuchs, M. Scheffler, S. Boeck, and J. Neugebauer, *Phys. Rev. B* **72**, 155317 (2005).

⁸F. Bechstedt, K. Seino, P. H. Hahn, and W. G. Schmidt, *Phys. Rev. B* **72**, 245114 (2005).

⁹H. Okumura, T. Koizumi, Y. Ishida, H. Yaguchi, and S. Yoshida, *Phys. Status Solidi B* **216**, 211 (1999).

¹⁰V. Cimalla, V. Lebedev, U. Kaiser, R. Goldhahn, C. Foerster, J. Pezoldt, and O. Ambacher, *Phys. Status Solidi C* **2**, 2199 (2005).

¹¹P. Schley, R. Goldhahn, C. Napierala, G. Gobsch, J. Schörmann, D. J. As, K. Lischka, M. Feneberg, and K. Thonke, *Semicond. Sci. Technol.* **23**, 055001 (2008).

¹²J. Schörmann, S. Potthast, D. J. As, and K. Lischka, *Appl. Phys. Lett.* **89**, 131910 (2006).

¹³V. Cimalla, J. Pezoldt, and O. Ambacher, *J. Phys. D: Appl. Phys.* **40**, 6386 (2007).

¹⁴T. Schupp, G. Rossbach, P. Schley, R. Goldhahn, K. Lischka, and D. J. As, *Phys. Status Solidi C* (to be published).

¹⁵C. Cobet, R. Goldhahn, W. Richter, and N. Esser, *Phys. Status Solidi B* **246**, 1440 (2009).

¹⁶R. Goldhahn, *Acta Phys. Pol. A* **104**, 123 (2003).

¹⁷R. Goldhahn, C. Buchheim, P. Schley, A. T. Winzer, and H. Wenzel, in *Nitride Semiconductor Devices: Principles and Simulation*, edited by J. Piprek (Wiley-VCH Verlag, Weinheim, 2007), p. 95.

¹⁸A. T. Winzer, G. Gobsch, R. Goldhahn, D. Fuhrmann, A. Hangleiter, A. Dadgar, and A. Krost, *Phys. Rev. B* **74**, 125207 (2006).

¹⁹R. A. R. Leute, M. Feneberg, R. Sauer, K. Thonke, S. B. Thapa, F. Scholz, Y. Taniyasu, and M. Kasu, *Appl. Phys. Lett.* **95**, 031903 (2009).

²⁰E. Martínez-Guerrero, F. Enjalbert, J. Barjon, E. Bellet-Almaric, B. Daudin, G. Ferro, D. Jalabert, L. S. Dang, H. Mariette, Y. Monteil, and G. Mula, *Phys. Status Solidi A* **188**, 695 (2001).

²¹M. P. Thompson, G. W. Auner, T. S. Zheleva, K. A. Jones, S. J. Simko, and J. N. Hilfiker, *J. Appl. Phys.* **89**, 3331 (2001).

²²L. X. Benedict, T. Wethkamp, K. Wilmers, C. Cobet, N. Esser, E. L. Shirley, W. Richter, and M. Cardona, *Solid State Commun.* **112**, 129 (1999).

²³J. Furthmüller, P. H. Hahn, F. Fuchs, and F. Bechstedt, *Phys. Rev. B* **72**, 205106 (2005).

²⁴S. Shokhovets, R. Goldhahn, G. Gobsch, S. Piekh, R. Lantier, A. Rizzi, V. Lebedev, and W. Richter, *J. Appl. Phys.* **94**, 307 (2003).

²⁵J. Ibáñez, S. Hernández, E. Alarcón-Lladó, R. Cuscó, L. Artús, S. V. Novikov, C. T. Foxon, and E. Calleja, *J. Appl. Phys.* **104**, 033544 (2008).